

Effects of Electron-Lattice Coupling on Charge Order in  $\theta$ -(ET) $_2$ XYasuhiro TANAKA<sup>1\*</sup> and Kenji YONEMITSU<sup>1,2</sup><sup>1</sup>*Institute for Molecular Science, Okazaki, Aichi 444-8585*<sup>2</sup>*Graduate University for Advanced Studies, Okazaki, Aichi 444-8585*

Charge ordering accompanied by lattice distortion in quasi-two dimensional organic conductors  $\theta$ -(ET) $_2$ X (ET=BEDT-TTF) is studied by using an extended Hubbard model with Peierls-type electron-lattice couplings within the Hartree-Fock approximation. It is found that the horizontal-stripe charge-ordered state, which is experimentally observed in  $\theta$ -(ET) $_2$ RbZn(SCN) $_4$ , is stabilized by the self-consistently determined lattice distortion. Furthermore, in the presence of the anisotropy in nearest-neighbor Coulomb interactions  $V_{ij}$ , the horizontal charge order becomes more stable than any other charge patterns such as diagonal, vertical and 3-fold-type states. At finite temperatures, we compare the free energies of various charge-ordered states and find a first-order transition from a metallic state with 3-fold charge order to the insulating state with the horizontal charge order. The role of lattice degrees of freedom in the realization of the horizontal charge order and the relevance to experiments on  $\theta$ -(ET) $_2$ X are discussed.

KEYWORDS: charge order, organic conductor, extended Hubbard model, electron-lattice coupling, Hartree-Fock approximation

Quasi-two-dimensional molecular conductors (ET) $_2$ X (ET=BEDT-TTF) show a variety of electronic phases at low temperatures.<sup>1,2</sup> Among them, charge order (CO) phenomena are one of the main subjects and have been intensively studied recently. (ET) $_2$ X is a member of the so-called 2:1 salts, which consists of alternating layers of anionic X<sup>-</sup> and cationic ET<sup>+1/2</sup> whose  $\pi$ -band is 3/4-filled. The variety of their physical properties originates from the spatial arrangements of ET molecules and strong Coulomb interaction among  $\pi$  electrons.

The experimental observations of CO are made in compounds such as  $\theta$ -(ET) $_2$ RbZn(SCN) $_4$ <sup>3,4</sup> and  $\alpha$ -(ET) $_2$ I $_3$ .<sup>5,6</sup>  $\theta$ -(ET) $_2$ RbZn(SCN) $_4$  shows a metal-insulator transition at  $T = 200$  K and a spin gap behavior at low temperatures.<sup>7</sup> The transition is of first order accompanied by lattice distortion. CO formation below  $T_c$  has been directly observed in NMR experiments.<sup>3,4</sup> Several experiments<sup>8-11</sup> such as Raman scattering<sup>9</sup> and X-ray scattering<sup>10,11</sup> measurements indicate that the horizontal-type CO is formed in this compound.

CO phenomena are considered to be a consequence of strong correlation effects among electrons, especially due to the long-range component of the Coulomb interaction. So far, many theoretical investigations on CO have been carried out from this point of view.<sup>12-19</sup> For example, Seo studied the extended Hubbard model, that includes both on-site ( $U$ ) and intersite ( $V$ ) Coulomb interactions using the Hartree approximation and discussed the stability of various stripe CO patterns in (ET) $_2$ X.<sup>12</sup> For  $\theta$ -type salts, the possibility of CO with long periodicity has been considered within the Hartree approximation.<sup>16</sup> Actually, X-ray experiments on  $\theta$ -(ET) $_2$ RbZn(SCN) $_4$  indicate a short-range CO with long periodicity in the metallic phase which is different from the horizontal stripe state at low temperatures.<sup>10,11</sup> A similar charge fluctuation is

observed in  $\theta$ -(ET) $_2$ CsZn(SCN) $_4$ , which shows coexisting charge modulations with different wave vectors without long-range order.<sup>20,21</sup>

On the other hand, a coupling between electron and lattice degrees of freedom also seems to have an important role. In fact, the CO transition is accompanied by a structural distortion in many  $\theta$ -type materials including  $\theta$ -(ET) $_2$ RbZn(SCN) $_4$ . Moreover, a particular role of structural modification at the transition is suggested by a recent observation of photoinduced melting of CO in  $\theta$ -(ET) $_2$ RbZn(SCN) $_4$  and  $\alpha$ -(ET) $_2$ I $_3$ .<sup>22</sup> Several theoretical studies<sup>12,13,16</sup> indicate that lattice effects indeed stabilize the horizontal CO in  $\theta$ -(ET) $_2$ X, although any electron-lattice coupling which causes structural change is not explicitly included in the calculations. Thus, it is important to investigate not only the role of electron-electron interactions but also lattice effects on CO.

In this paper, we study the CO transition and lattice distortion in  $\theta$ -(ET) $_2$ RbZn(SCN) $_4$  by using the extended Hubbard model with Peierls-type electron-lattice couplings within the Hartree-Fock approximation. Figures 1(a) and 1(b) show the structures of  $\theta$ -(ET) $_2$ RbZn(SCN) $_4$  in the metallic and insulating phases, which is called  $\theta$ -type and  $\theta_d$ -type, respectively. At  $T > T_c$ , the unit cell contains two molecules and two kinds of transfer integrals,  $t_c$  and  $t_p$ . On the other hand, six transfer integrals exist in the unit cell with a doubled  $c$ -axis at  $T < T_c$ . Since the displacements of ET molecules and the resulting change in transfer integrals are rather complicated,<sup>10</sup> here we study the effects of electron-lattice couplings which cause the modulations of transfer integrals that are experimentally observed [Fig. 1(b)], and do not consider any other electron-lattice couplings. This leads to three kinds of interactions between electrons and the lattice degrees of freedom: transfer integrals modulated by  $c$ - and  $a$ -axis molecular translations and rotation, as deduced from the results of the X-ray experiment.<sup>10</sup> For

\*E-mail address: yasuihiro@ims.ac.jp

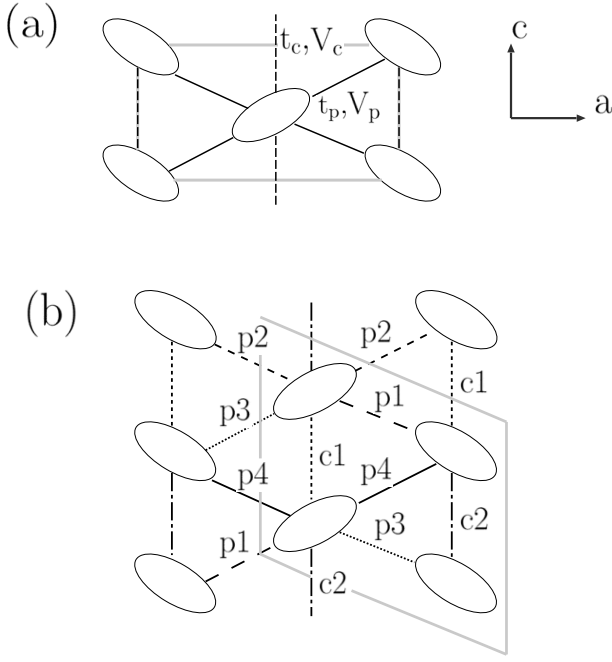


Fig. 1. Schematic representation of (a)  $\theta$ -type and (b)  $\theta_d$ -type structures. The gray solid lines indicate the unit cell. The values of transfer integrals in (b) from the extended Hückel method are as follows,  $t_{c1} = 1.5$ ,  $t_{c2} = 5.2$ ,  $t_{p1} = 16.9$ ,  $t_{p2} = -6.5$ ,  $t_{p3} = 2.2$ , and  $t_{p4} = -12.3(10^{-2}\text{eV})$ .

simplicity, these electron-lattice couplings are assumed to be independent of each other. First, the  $c$ -axis translation alternates  $t_c$  and gives  $t_{c1}$  and  $t_{c2}$  in Fig. 1(b). This is indeed expected since the length of the  $t_{c1}$  bond increases while that of the  $t_{c2}$  bond decreases through the CO transition.<sup>10, 23, 24</sup> On the other hand, we observe that the length of the  $t_{p1}$  bond decreases while that of the  $t_{p3}$  bond increases,<sup>10, 24</sup> from which the modulations of  $t_{p1}$  and  $t_{p3}$  can be regarded as due to the  $a$ -axis translation. However, a similar consideration does not hold for the changes of  $t_{p2}$  and  $t_{p4}$ . In fact, the experimental estimation of transfer integrals indicates that rotational degrees of freedom are important. It shows that the dependences of the transfer integrals on relative angles (called elevation angles<sup>10</sup>) of ET molecules are large and allow the transfer integrals  $|t_{p2}|$  ( $|t_{p4}|$ ) on the horizontally connected bonds to uniformly decrease (increase), as can be seen from Fig. 1(b). In the actual compound, this type of modulation seems to be important since the horizontal CO is formed by the  $t_{p4}$  chains with hole-rich molecules and the  $t_{p2}$  chains with hole-poor molecules. Therefore, in the present study, we simply introduce such rotational degrees of freedom in order to take account of the experimentally observed modulations of  $t_{p2}$  and  $t_{p4}$ , which are difficult to understand from a molecular translation.

Our Hamiltonian is then written as

$$H = \sum_{\langle ij \rangle \sigma} (t_{i,j} + \alpha_{i,j} u_{i,j}) (c_{i\sigma}^\dagger c_{j\sigma} + \text{h.c.}) + U \sum_i n_{i\uparrow} n_{i\downarrow} + \sum_{\langle ij \rangle} V_{i,j} n_i n_j + \sum_{\langle ij \rangle} \frac{K_{i,j}}{2} u_{i,j}^2, \quad (1)$$

where  $\langle ij \rangle$  represents the summation over pairs of neigh-

boring sites,  $c_{i\sigma}^\dagger (c_{i\sigma})$  denotes the creation (annihilation) operator for an electron with spin  $\sigma$  at the  $i$ th site,  $n_{i\sigma} = c_{i\sigma}^\dagger c_{i\sigma}$ , and  $n_i = n_{i\uparrow} + n_{i\downarrow}$ . The transfer integral  $t_{ij}$  means  $t_c$  or  $t_p$  in the  $\theta$ -type structure. The electron-lattice coupling constant, the lattice translational or rotational displacement and the elastic constant are denoted by  $\alpha_{i,j}$ ,  $u_{i,j}$ , and  $K_{i,j}$ , respectively. The electron density is  $3/4$ -filled and we consider nearest-neighbor Coulomb interactions  $V_c$  for the vertical direction and  $V_p$  for the diagonal direction as shown in Fig. 1(a). For the lattice degrees of freedom, we further introduce new variables as  $y_{i,j} = \alpha_{i,j} u_{i,j}$  and  $s_{i,j} = \alpha_{i,j}^2 / K_{i,j}$ , where  $s_{i,j}$  is written as  $s_c$ ,  $s_a$  and  $s_\phi$  for  $c$ -axis translation,  $a$ -axis translation and rotation, respectively, as discussed above. Similarly, we can rewrite  $y_{ij}$  by using the subscripts  $c$ ,  $a$  and  $\phi$ , and as a result the transfer integrals

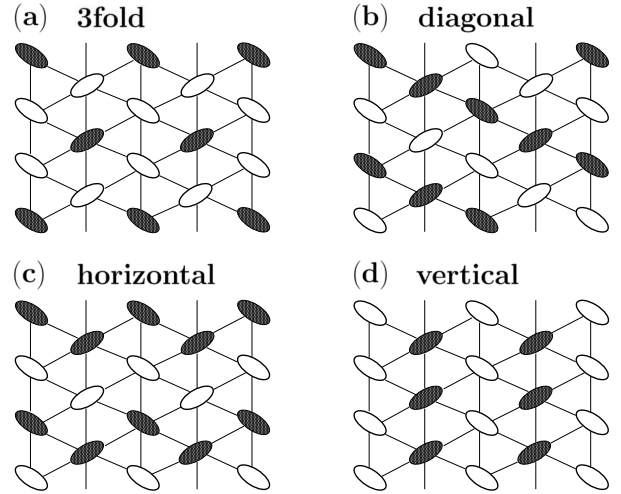


Fig. 2. Order parameters considered in the Hartree-Fock approximation. The hole-rich and -poor sites are represented by the solid and open ellipses, respectively.

in the distorted structure are given by

$$\begin{aligned} t_{c1} &= t_c + y_c, \quad t_{c2} = t_c - y_c, \\ t_{p1} &= t_p + y_a, \quad t_{p2} = t_p - y_\phi, \\ t_{p3} &= t_p - y_a, \quad t_{p4} = t_p + y_\phi. \end{aligned} \quad (2)$$

Note that the signs in eq. (2) are chosen so that the resulting transfer integrals correspond with the experimental ones if  $y_l > 0$  for  $l = c, a$  and  $\phi$ .<sup>25</sup>

We apply the Hartree-Fock approximation,

$$\begin{aligned} n_{i\sigma} n_{j\sigma'} &\rightarrow \langle n_{i\sigma} \rangle n_{j\sigma'} + n_{i\sigma} \langle n_{j\sigma'} \rangle - \langle n_{i\sigma} \rangle \langle n_{j\sigma'} \rangle \\ &- \langle c_{i\sigma}^\dagger c_{j\sigma'} \rangle c_{j\sigma'}^\dagger c_{i\sigma} - c_{i\sigma}^\dagger c_{j\sigma'} \langle c_{j\sigma'}^\dagger c_{i\sigma} \rangle \\ &+ \langle c_{i\sigma}^\dagger c_{j\sigma'} \rangle \langle c_{j\sigma'}^\dagger c_{i\sigma} \rangle, \end{aligned} \quad (3)$$

to eq. (1) and diagonalize the obtained Hamiltonian in  $k$ -space by assuming the unit cell of each mean-field order parameter. We use four types of CO order parameters with respect to charge degrees of freedom, which are shown in Fig. 2. As for the spin degrees of freedom, we consider three spin configurations in each stripe-type

CO which are identical to those of ref. 12. For the 3-fold CO, spin alternation between the hole-rich and -poor sites is considered. The ground-state energy is calculated by solving the mean-field equation self-consistently with the lattice displacements, which are determined by the Hellmann-Feynman theorem  $\langle \frac{\partial H}{\partial y_l} \rangle = 0$ , where  $y_l$  means  $y_c$ ,  $y_a$  or  $y_\phi$ . The energy per site is given by

$$E = \frac{1}{N} \left( \sum_{l\mathbf{k}\sigma} E_{l\mathbf{k}\sigma} n_F(E_{l\mathbf{k}\sigma}) - U \sum_i \langle n_{i\uparrow} \rangle \langle n_{i\downarrow} \rangle - \sum_{\langle ij \rangle} V_{ij} \langle n_i \rangle \langle n_j \rangle + \sum_{\langle ij \rangle \sigma} V_{ij} \langle c_{i\sigma}^\dagger c_{j\sigma} \rangle \langle c_{j\sigma}^\dagger c_{i\sigma} \rangle + \sum_{\langle ij \rangle} \frac{y_{ij}^2}{2s_{ij}} \right), \quad (4)$$

where  $l$ ,  $E_{l\mathbf{k}\sigma}$  and  $n_F$  are the band index, the energy eigenvalue of the mean-field Hamiltonian and the Fermi distribution function, respectively.  $N$  is the total number of sites. In the following, we set  $t_p = 0.1$  eV,  $t_c = -0.04$  eV, and  $U = 0.7$  eV. The ratio  $V_c/U$  is fixed at 0.35 and the anisotropy in nearest-neighbor Coulomb interactions  $V_p/V_c$  is treated as a parameter.

The ground-state energies of various CO patterns per site as a function of  $V_p/V_c$  are compared in Fig. 3, where the energy of the 3-fold CO is set at zero. We have shown only the lowest-energy state of each CO pattern with different spin configurations. In the absence of an electron-lattice coupling, the 3-fold CO with a ferrimagnetic spin configuration is the most favorable in the nearly isotropic region, i.e.,  $V_p/V_c \sim 1$ . On the other hand, the diagonal CO whose spin configuration is antiferromagnetic along the stripe and between stripes on the  $c$ -axis is stable when  $V_p/V_c$  is small. These features are consistent with the previous study.<sup>16</sup> For the horizontal CO, we plotted the energy of the state which is antiferromagnetic along the stripe and ferromagnetic between stripes on the  $c$ -axis. Note that the state which is antiferromagnetic on the  $c$ -axis has a close energy and is nearly degenerate with the above state. As can be seen from Fig. 3, there is no region where the horizontal CO has the lowest energy in the absence of an electron-lattice coupling.

However, in the presence of the electron-lattice couplings, the horizontal CO becomes more stable owing to the lattice distortions. The values of the electron-lattice couplings are chosen at  $s_c = 0.08$ ,  $s_a = 0.17$  and  $s_\phi = 0.11$  to obtain realistic values of lattice displacements. The horizontal CO has hole-rich sites on the  $t_{p4}$  chains, which is consistent with the experiments. The energy gain mainly comes from the difference between  $t_{p2}$  and  $t_{p4}$ . This is reasonable since the horizontal CO can be stabilized by the exchange coupling between neighboring spins on the stripes. Although the diagonal CO is not affected by any electron-lattice coupling, the vertical and 3-fold COs also have energy gain from the lattice modulation. The energy of the vertical CO is lowered by  $s_a$ . On the other hand, that of the 3-fold CO is lowered by  $s_c$  and  $s_\phi$ . In this state, there is a weak horizontal charge modulation caused by the lattice distortion in the background of the 3-fold CO. Note that the 3-fold CO is metallic even

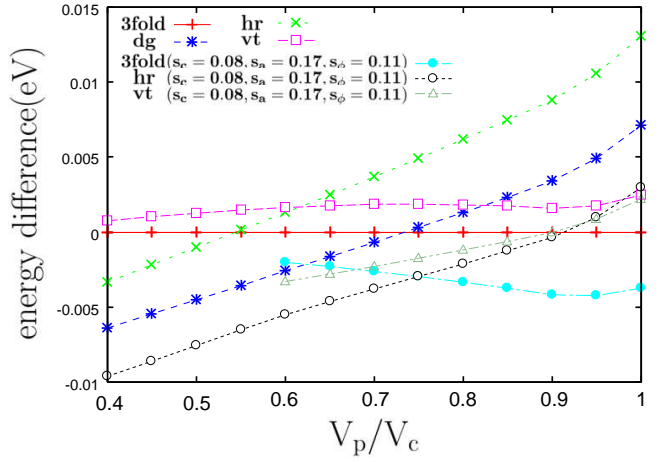


Fig. 3. (Color online) Relative energies as a function of anisotropy  $V_p/V_c$ , where the energy of the 3-fold state is chosen to be zero. dg, hr and vt are abbreviations of diagonal, horizontal and vertical COs, respectively.

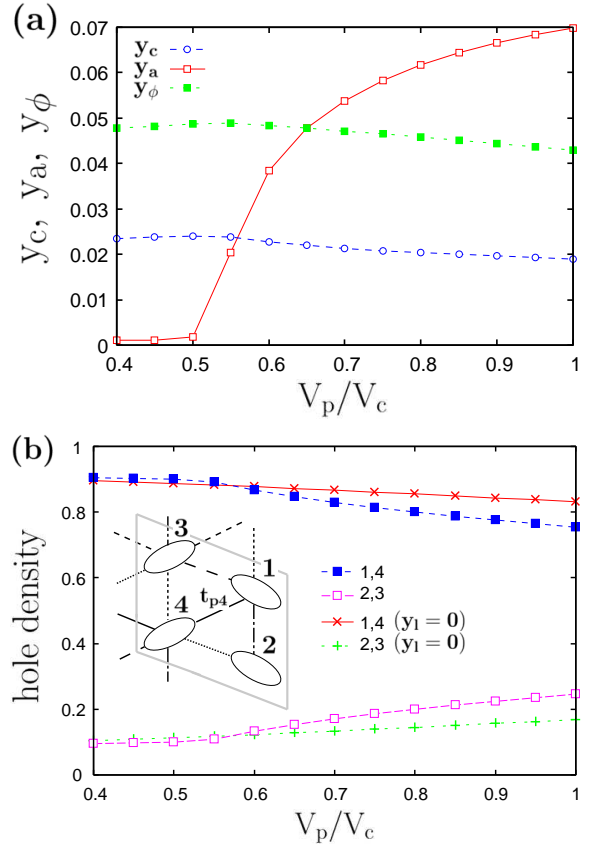


Fig. 4. (Color online) (a) Modulations of transfer integrals and (b) hole density at each site in the horizontal CO. In (b), the hole densities in the absence of an electron-lattice coupling are also shown.

if the transfer integrals are modulated, whereas the horizontal CO is insulating. As a result, the horizontal CO with lattice distortion becomes stable for  $V_p/V_c < 0.75$ , while the 3-fold CO is favorable for  $V_p/V_c > 0.75$ , as shown in Fig. 3.

In Fig. 4, we show the modulations of the transfer in-

tegrals and the hole density at each site in the case of the horizontal CO. Although  $y_c$  and  $y_\phi$  distortions do not depend so much on  $V_p/V_c$ , the  $y_a$  distortion increases with  $V_p/V_c$ . It becomes largest for  $V_p/V_c \geq 0.7$ . In fact, the former two electron-lattice couplings favor the horizontal CO while the latter tends to decrease the order parameter as seen from Fig. 4(b), although the energy is lowered. Experimentally, the difference between  $t_{p1}$  and  $t_{p3}$  is the largest while that between  $t_{c1}$  and  $t_{c2}$  is the smallest. Our result seems to be consistent with the experimental one for  $V_p/V_c \sim 0.7$ . The detailed role of each electron-lattice coupling on the horizontal CO is discussed elsewhere.<sup>26</sup>

Next, we consider the stability of these COs at finite temperatures by calculating the free energy within the Hartree-Fock approximation. The free energy per site is written as

$$F = \frac{1}{N} \left( \mu N_{tot} - \frac{1}{\beta} \sum_{l\mathbf{k}\sigma} \ln(1 + \exp\{-\beta(E_{l\mathbf{k}\sigma} - \mu)\}) \right. \\ \left. - U \sum_i \langle n_{i\uparrow} \rangle \langle n_{i\downarrow} \rangle - \sum_{\langle ij \rangle} V_{ij} \langle n_i \rangle \langle n_j \rangle \right. \\ \left. + \sum_{\langle ij \rangle \sigma} V_{ij} \langle c_{i\sigma}^\dagger c_{j\sigma} \rangle \langle c_{j\sigma}^\dagger c_{i\sigma} \rangle + \sum_{\langle ij \rangle} \frac{y_{ij}^2}{2s_{ij}} \right), \quad (5)$$

where  $\mu$ ,  $N_{tot}$  and  $\beta$  are the chemical potential, the total number of electrons and the inverse temperature, respectively. The phase diagram on the  $(T, V_p/V_c)$  plane, which is obtained by comparing the free energies of different CO patterns, is shown in Fig. 5. The values of the electron-lattice couplings are the same as those used for  $T = 0$ . For  $V_p/V_c \sim 1$ , the 3-fold state with lattice distortion

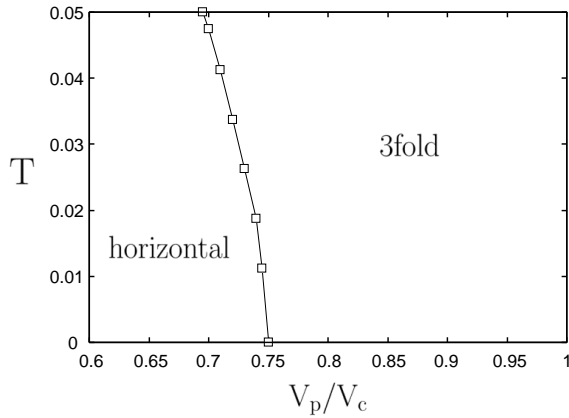


Fig. 5. Phase diagram on  $(T, V_p/V_c)$  plane in the presence of electron-lattice coupling.

has the lowest free energy for a wide temperature range. On the other hand, the horizontal CO is the most stable for  $V_p/V_c < 0.7$ . There is a first-order metal-insulator transition from the 3-fold CO to the horizontal CO near  $V_p/V_c = 0.7$ . For the parameters we used, the normal metallic state with a uniform charge density always has a higher free energy than the 3-fold CO because of the large Coulomb interactions. We note that if we choose smaller values of  $U$  and  $V_{ij}$ , the diagonal CO, which is

undistorted even with electron-lattice couplings, is more stable than the horizontal CO. Therefore, large Coulomb interactions seem to be important to stabilize the horizontal CO with realistic values of the lattice distortions. In fact, the energy gain of the horizontal CO due to the lattice distortions can be understood by the perturbational calculations from the strong coupling limit, i.e.,  $t_{ij} = 0$ .<sup>27</sup>

Finally, we discuss the relevance of the results to the experiments and relations to other theoretical studies. The stabilization of the horizontal CO due to the lattice distortion is consistent with the experiments on  $\theta$ -(ET)<sub>2</sub>RbZn(SCN)<sub>4</sub>. Since the horizontal CO does not become the ground state without electron-lattice coupling, the effects of the lattice distortion are considered to be crucial in realizing the horizontal CO in the present model. This result is also qualitatively consistent with the recent exact-diagonalization study<sup>27</sup> for eq. (1) on small clusters. Moreover, the first-order metal-insulator transition at a finite temperature can be related to the experimental results of this compound, although the obtained wave vector of the charge modulation at high temperatures is different from that of the experiments in the metallic phase. It has recently been pointed out that longer range than the nearest-neighbor Coulomb interactions can reproduce the experimental observation.<sup>18</sup> As for the spin degrees of freedom, both the 3-fold and horizontal COs in our Hartree-Fock calculation have spin orders which have not been observed in the experiments. It is considered that the effect of quantum fluctuation is necessary in discussing the behavior of the spin degrees of freedom.<sup>16</sup>

The previous estimations of the intersite Coulomb interactions  $V_p$  and  $V_c$  show that these values are comparable,  $V_p/V_c \sim 1$ ,<sup>14</sup> where the 3-fold CO is the most stable in our calculation. A variational Monte Carlo study<sup>17</sup> in the absence of an electron-lattice coupling also shows that the 3-fold CO is stable for  $V_p/V_c \sim 1$ . According to the recent exact-diagonalization study,<sup>27</sup> the horizontal CO with lattice distortion becomes more stable even at  $V_p/V_c \sim 1$  if we take account of quantum fluctuations that are neglected in the Hartree-Fock approximation. An exact-diagonalization study<sup>13</sup> also indicates that the Holstein-type electron-lattice coupling stabilizes the horizontal CO.

At the nearly isotropic region  $V_p/V_c \sim 1$ , we find that the 3-fold state with a coexisting weak horizontal charge modulation is stable. This result can be related to the X-ray experiments on  $\theta$ -(ET)<sub>2</sub>CsZn(SCN)<sub>4</sub>,<sup>20,21</sup> which shows two types of COs coexisting as short-range fluctuations. Although the present Hartree-Fock calculation gives a long-range CO, it is natural to expect that the effect of fluctuations can destroy the long-range order and results in a state such that two types of COs coexist as short-range fluctuations.

In summary, we investigated the effects of Peierls-type electron-lattice couplings on the CO in  $\theta$ -(ET)<sub>2</sub>X by using the extended Hubbard model through the Hartree-Fock approximation. We found that the horizontal stripe CO which is observed in the experiments is stabilized by the lattice distortion. Moreover, at finite temperatures,



there is a first-order metal-insulator transition in the presence of the anisotropy in  $V_{ij}$ , which can be related to the phase transition in  $\theta$ -(ET)<sub>2</sub>RbZn(SCN)<sub>4</sub>. These results show that the lattice effect plays an important role on the CO phenomena in  $\theta$ -(ET)<sub>2</sub>X.

### Acknowledgment

The authors would like to thank H. Seo and S. Miyashita for helpful discussions. This work was supported by Grants-in-Aid and the Next Generation Super Computing Project, Nanoscience Program, from the Ministry of Education, Culture, Sports, Science and Technology, Japan.

- 1) T. Ishiguro, K. Yamaji, and G. Saito: *Organic Superconductors*, (Springer-Verlag, Berlin, 1998) 2nd ed.
- 2) H. Seo, C. Hotta, and H. Fukuyama: Chem. Rev. **104** (2004) 5005.
- 3) K. Miyagawa, A. Kawamoto, and K. Kanoda: Phys. Rev. B **62** (2000) 7679.
- 4) R. Chiba, H. Yamamoto, T. Takahashi, and T. Nakamura: J. Phys. Chem. Solids. **62** (2001) 389.
- 5) Y. Takano, K. Hiraki, H. M. Yamamoto, T. Nakamura, and T. Takahashi: J. Phys. Chem. Solids **62** (2001) 393.
- 6) Y. Takano, K. Hiraki, H. M. Yamamoto, T. Nakamura, and T. Takahashi: Synth. Met. **120** (2001) 1081.
- 7) H. Mori, S. Tanaka, and T. Mori: Phys. Rev. B **57** (1998) 12023.
- 8) H. Tajima, S. Kyoden, H. Mori, and S. Tanaka: Phys. Rev. B **62** (2000) 9378.
- 9) K. Yamamoto, K. Yakushi, K. Miyagawa, K. Kanoda, and A. Kawamoto: Phys. Rev. B **65** (2002) 085110.
- 10) M. Watanabe, Y. Noda, Y. Nogami, and H. Mori: J. Phys. Soc. Jpn. **73** (2004) 116.
- 11) M. Watanabe, Y. Noda, Y. Nogami, and H. Mori: J. Phys. Soc. Jpn. **74** (2005) 2011.
- 12) H. Seo: J. Phys. Soc. Jpn. **69** (2000) 805.
- 13) R. T. Clay, S. Mazumdar, and D. K. Campbell: J. Phys. Soc. Jpn. **71** (2002) 1816.
- 14) T. Mori: J. Phys. Soc. Jpn. **72** (2003) 1469.
- 15) J. Merino, H. Seo, and M. Ogata: Phys. Rev. B **71** (2005) 125111.
- 16) M. Kaneko and M. Ogata: J. Phys. Soc. Jpn. **75** (2006) 014710.
- 17) H. Watanabe and M. Ogata: J. Phys. Soc. Jpn. **75** (2006) 063702.
- 18) K. Kuroki: J. Phys. Soc. Jpn. **75** (2006) 114716.
- 19) C. Hotta, N. Furukawa, A. Nakagawa, and K. Kubo: J. Phys. Soc. Jpn. **75** (2006) 123704.
- 20) M. Watanabe, Y. Nogami, K. Oshima, H. Mori, and S. Tanaka: J. Phys. Soc. Jpn. **68** (1999) 2654.
- 21) Y. Nogami, J.-P. Pouget, M. Watanabe, K. Oshima, H. Mori, S. Tanaka and T. Mori: Synth. Met. **103** (1999) 1911.
- 22) S. Iwai, K. Yamamoto, A. Kashiwazaki, F. Hiramatsu, H. Nakaya, Y. Kawakami, K. Yakushi, H. Okamoto, H. Mori, and Y. Nishio: Phys. Rev. Lett. **98** (2007) 097402.
- 23) Here, the length of the bond means the distance between the geometrical centers of two molecules.
- 24) M. Watanabe: private communication.
- 25) In the present study, we choose  $t_p > 0$  and  $t_c < 0$ . In this choice, a correspondence with the experimental values of transfer integrals in the low-temperature phase is obtained since we can change the signs of  $t_{c1}$ ,  $t_{c2}$ ,  $t_{p2}$  and  $t_{p4}$  simultaneously by the redefinition of electron operators.
- 26) Y. Tanaka and K. Yonemitsu: in preparation.
- 27) S. Miyashita and K. Yonemitsu: in preparation.